Ammonia Gas Sensing Properties of Gold- and Silver-Modified Tin Dioxide Thin Films

Asaad Ahmad Kamil[1], Nabeel Ali Bakr[1], Tahseen Hussain Mubarak[1], Jasim Al-Zanganawee[1], Ziad Tariq Khodair[1] and Kiran Dasharath Diwate[2]

[1]*Department of Physics, College of Science, University of Diyala, 32001 Baqubah, Iraq*

[2]*Department of Physics, School of Basic and Applied Sciences, JSPM University, 412207 Pune, India*

prof.asaad@uodiyala.edu.iq, nabeelalibakr@yahoo.com, {prof.dr.tahseen, aLzanganawee}@uodiyala.edu.iq, ziad_tariq70@yahoo.com, kdd@jspmuni.ac.in

Keywords: Spin Coating, SnO_2 Structural & Optical Properties, Au NPs, Ag NPs, NH_3 Gas Sensing.

Abstract: In this work, SnO_2 thin films were fabricated on quartz substrates using the sol–gel spin-coating method. The films were successfully prepared through multiple coating cycles to study the influence of deposition repetition on film properties. Tin(II) chloride dihydrate ($SnCl_2 \cdot 2H_2O$) served as the precursor material, 2-methoxyethanol was used as the solvent, and monoethanolamine (MEA) acted as the stabilizing agent. Gold (Au) and silver (Ag) nanoparticles were synthesized separately using the pulsed laser ablation in liquid (PLAL) technique with a Q-switched Nd: YAG laser operating at 1064 nm wavelength, 520 mJ pulse energy, 1 Hz repetition rate, and 450 pulses. The SnO_2 precursor solution was then mixed with the Au and Ag colloids in volumetric ratios of 3:2 and 4:1, respectively. The surface morphology of the resulting nanocomposite films was analyzed using field emission scanning electron microscopy (FE-SEM), while their optical characteristics were examined via UV–Vis spectroscopy. X-ray diffraction (XRD) patterns revealed six principal peaks: four at (110), (101), (211), and (112), which correspond to the tetragonal rutile phase of SnO_2, and two additional peaks at (200) and (220), attributed to the cubic crystalline phases of Au and Ag nanoparticles. A shared (111) reflection was also detected for both SnO_2 and the metallic nanoparticles. Optical studies demonstrated a reduction in the band-gap energy (3.85–3.56 eV) with increasing concentrations of Au and Ag nanoparticles within the SnO_2 matrix. Among all samples, the SnO_2+Au (3:2) composite exhibited the best NH_3 gas-sensing performance, exhibiting high sensitivity with rapid response and recovery times. The optimum operating temperature of 300 °C, at which the best gas-sensing response was observed.

1 INTRODUCTION

Tin oxide (SnO_2) is currently one of the most extensively studied materials owing to its remarkable physical and chemical characteristics. It is a well-known n-type semiconductor possessing a wide band gap of 3.6–3.8 eV [1] – [3] and crystallizes in a tetragonal rutile structure with lattice parameters a = b = 4.737 Å, c = 3.826 Å, and $\alpha = \beta = \gamma = 90°$.

Owing to its transparency and favorable electrical properties, SnO_2 thin films have been employed in a variety of devices, including gas sensors and aerospace applications [4]. Furthermore, they play an important role in solar cells [5], [6], transparent conducting electrodes [7], and catalytic systems [8].

The performance of SnO_2 in these applications is strongly influenced by its structural characteristics; for instance, its gas-sensing efficiency is highly dependent on the particle size and specific surface area [9], [10].

Noble metal nanoparticles (NPs) such as silver (Ag) and gold (Au) have attracted substantial interest because of their exceptional electrical, optical, physical, chemical, and magnetic properties [11]. Gold and silver NPs exhibit pronounced surface plasmon resonance (SPR) in the green-to-red region of the UV–visible spectrum, resulting from photon absorption and scattering.

These nanoparticles display excellent stability under chemical, thermal, and photonic conditions and are known for their catalytic activity and biocompatibility.

Silver nanoparticles have been widely applied in nanosensors, catalysis, optical data storage, antibacterial coatings, and environmental

technologies, as well as in food preservation, textile treatments, and medical applications.

Additionally, they serve as biological markers and are used in electroluminescent devices [12]. Similarly, gold nanoparticles exhibit size-dependent properties that make them useful in immunohistochemistry, optical microscopy (including TEM), environmental detection, drug delivery, biomarker identification, chemical sensing, and DNA analysis [12].

The present work aims to study the influence of incorporating Au and Ag nanoparticles into SnO_2 thin films synthesized via the sol–gel spin-coating technique. The focus is on examining how these metallic nanoparticles affect the morphological, structural, and optical properties of the films and on evaluating their potential gas-sensing performance.

2 EXPERIMENTAL PROCEDURES

Thin layers of SnO_2 were deposited onto quartz substrates using the sol–gel spin-coating technique. The precursor solution was prepared from tin (II) chloride dihydrate ($SnCl_2 \cdot 2H_2O$) as the starting material, 2-methoxyethanol as the solvent, and monoethanolamine (MEA) as the stabilizing agent.

A 0.5 M $SnCl_2 \cdot 2H_2O$ solution was obtained by dissolving 0.5641 g of the salt in 5 mL of 2-methoxyethanol. The resulting mixture was continuously stirred and gently heated at 60 °C for 1 hour to form a homogeneous and transparent sol.

Gold (Au) and silver (Ag) nanoparticles were synthesized using the pulsed laser ablation in liquid (PLAL) method, employing Nd:YAG laser system (HUAFEI, China) operated at pulse energy of 520 mJ, wavelength of 1064 nm, 450 pulses, and repetition rate of 1 Hz.

Prior to ablation, pure gold and Ag metal targets were thoroughly cleaned with 99.999% ethyl alcohol to eliminate organic contaminants and dust. The targets were then immersed in 5 mL of 2-methoxyethanol, maintaining a distance of 60 mm between the target surface and the laser lens [13].

To prepare the nanocomposite sols, the SnO_2 precursor solution was mixed with Au and Ag colloidal suspensions in volumetric ratios of 4:1 and 3:2. The deposition of multilayer SnO_2:Au as well as SnO_2:Ag thin films was carried out using a spin-coating system (Ossila, UK) operated at 3000 rpm for 30 seconds.

After each coating, the samples were pre-dried on a hot plate at 150 °C for ~15 minutes in ambient conditions. The process was repeated to produce uniform films with the required thickness. Then The films were heat-treated at ~400 °C for one hour in a muffle furnace to improve their crystallinity and substrate adhesion.

The morphology and elemental composition of the films were examined by FE-SEM (TESCAN MIRA3, Czech Republic). Structural studies were conducted using Low-Angle XRD (Bruker D8 Advance, Germany) equipped with a CuKα radiation source operating at 30 mA and 40 kV. Optical absorbance spectra were measured using UV–Vis spectrometer (UV - 1800, Shimadzu, Japan).

The gas sensing properties were evaluated using SnO_2-based sensors fabricated on glass substrates. Measurements were performed at different operating temperatures (150, 200, 250, and 300 °C) under exposure to reducing NH_3 gas (30 ppm) environment.

3 RESULTS AND DISCUSSION

3.1 FE-SEM Analysis

The morphology of pure SnO_2, SnO_2+Au (3:2), SnO_2+Au (4:1), SnO_2+Ag (3:2), and SnO_2+Ag (4:1) thin films grown on quartz substrates was analyzed using Field Emission Scanning Electron Microscopy (FE-SEM).

Figure 1 presents the FE-SEM micrographs of 0.5 M SnO_2 thin films recorded at a magnification of 150 KX and a scale of 200 nm. The obtained images demonstrate a uniform and homogeneous surface morphology, indicating an even distribution of SnO_2 nanoparticles throughout the examined area.

The particles display a nearly spherical geometry with slight variation in grain size but maintain a narrow size distribution. Additionally, the micrographs reveal the presence of smaller nanoparticles occupying the interstitial spaces between larger grains, allowing for a densely packed structure [14], [15]. The particle size of SnO_2 thin film, estimated using ImageJ software, was ~16.3 nm.

Figures 2A and 2B display the FE-SEM micrographs captured at a magnification of 50 KX for SnO_2+Au (3:2) and SnO_2+Au (4:1) thin films respectively. The images indicate that most of the nanoparticles exhibit a nearly spherical morphology, and a noticeable agglomeration can be observed, which arises from the small particle size.

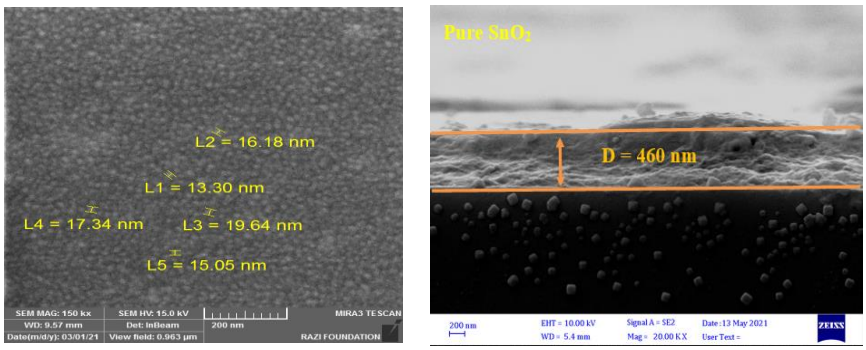

Figure 1: FE-SEM image of SnO_2 thin films at magnification of 150 KX and cross–section image.

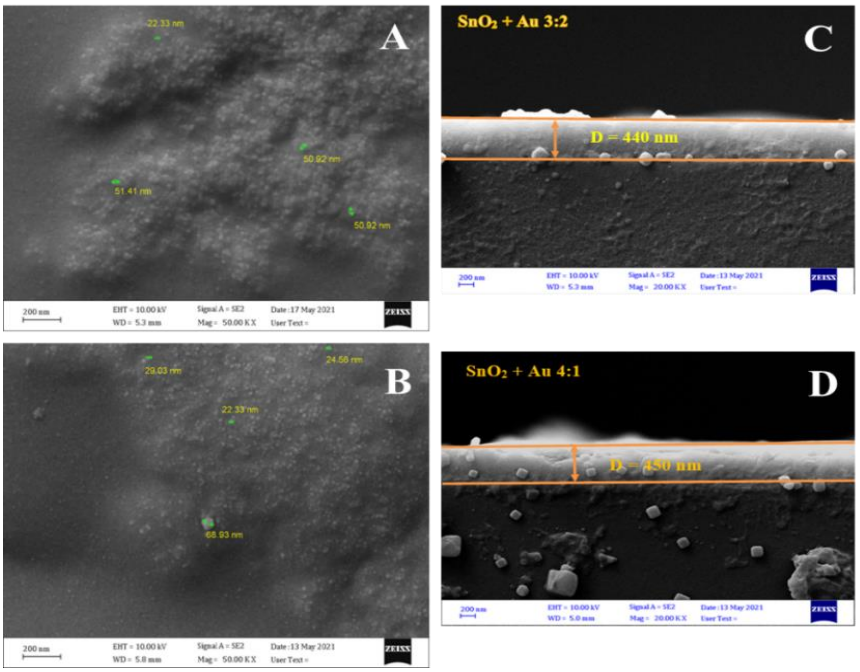

Figure 2: FE-SEM analysis for SnO_2 incorporated with Au NPs (A) SnO_2 +Au (3:2) (B) SnO_2 +Au (4:1), (C) and (D) Cross –section images.

This agglomeration tendency becomes more pronounced as the particle size decreases due to the enhanced interparticle attraction forces that promote clustering [16]. The average particle sizes were found to be approximately 43.89 nm for SnO_2+Au (3:2) and 36.21 nm for SnO_2+Au (4:1), respectively.

The film thickness determined from cross-sectional micrographs was measured to be 440 nm for SnO_2+Au (3:2) (see Fig. 2C) and 450 nm for SnO_2+Au (4:1) (see Fig. 2D).

Figures 3A and 3B present the FE-SEM micrographs of SnO_2 thin films incorporated with Ag nanoparticles (NPs) at two different volumetric ratios: (A) SnO_2+Ag (3:2) and (B) SnO_2+Ag (4:1).

The images, recorded at 50 KX magnification, reveal randomly distributed nanoparticles with irregular shapes and variable grain sizes, although many grains exhibit a nearly spherical structure.

Noticeable agglomeration of ultrafine nanoparticles is observed on the surface of larger grains, indicating particle clustering during film growth [16], [17]. The average particle sizes were determined to be approximately 72.32 nm for SnO_2+Ag (3:2) and 79.63 nm for SnO_2+Ag (4:1). The increase in particle size for the SnO_2+Ag (4:1) film is attributed to the higher concentration of silver nanoparticles, which promotes surface coalescence. The film thickness, estimated from the cross-sectional images, was about 440 nm for SnO_2+Ag (3:2) (see Fig. 3C) and 460 nm for SnO_2+Ag (4:1) (see Fig. 3D).

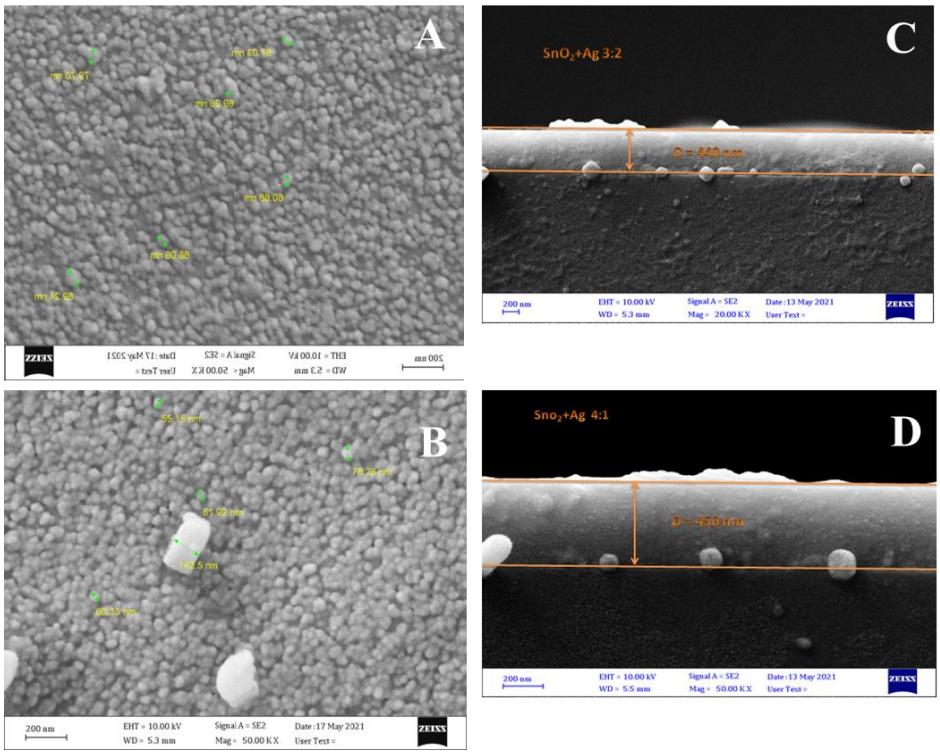

Figure 3: FE-SEM analysis for SnO_2 incorporated with Ag NPs. (A) SnO_2 +Ag(3:2) (B) SnO_2 +Ag(4:1), (C) and (D) Cross –section images.

3.2 X-ray Diffraction Results

The X-ray diffraction patterns of SnO_2 films incorporated with Au and Ag nanoparticles were analyzed using low-angle X-ray diffraction, and the results are shown in Figure 4.

Six main diffraction peaks were observed. Four of them, corresponding to the (110), (101), (211), and (112) planes, confirm the formation of SnO_2 with a tetragonal rutile crystal structure. The remaining two peaks, associated with the (220) and (200) planes, are attributed to Au and Ag nanoparticles, indicating their cubic crystal structure.

In addition, a distinct reflection was observed that can be associated with both SnO_2 and Au/Ag crystal planes, in agreement with standard reference data (JCPDS 41-1445 for SnO_2 and JCPDS 04-0784 for Au and 04-0783 for Ag). For the SnO_2–Ag composite films, an additional diffraction peak appeared corresponding to the AgO phase with a (111) orientation, consistent with JCPDS 03-5662. The diffraction peaks are sharp but relatively low in intensity, which confirms the nanocrystalline nature of the films.

With increasing concentration of Au and Ag nanoparticles, the diffraction peaks become more pronounced, indicating improved crystallinity. The most intense reflections are observed near 26.52° and 38.33°, which are assigned to the (110) and (111) planes related to SnO_2, Au, and Ag phases [14], [17].

The crystallite size of the prepared samples was estimated using the standard approach based on X-ray peak broadening, where it depends on the X-ray wavelength, peak width, and diffraction angle [18,19]. The lattice parameters were evaluated assuming a tetragonal crystal structure using interplanar spacing relationships that relate lattice constants to crystallographic indices [20]. All structural parameters, including interplanar spacing values, are summarized in Tables 1 and 2.

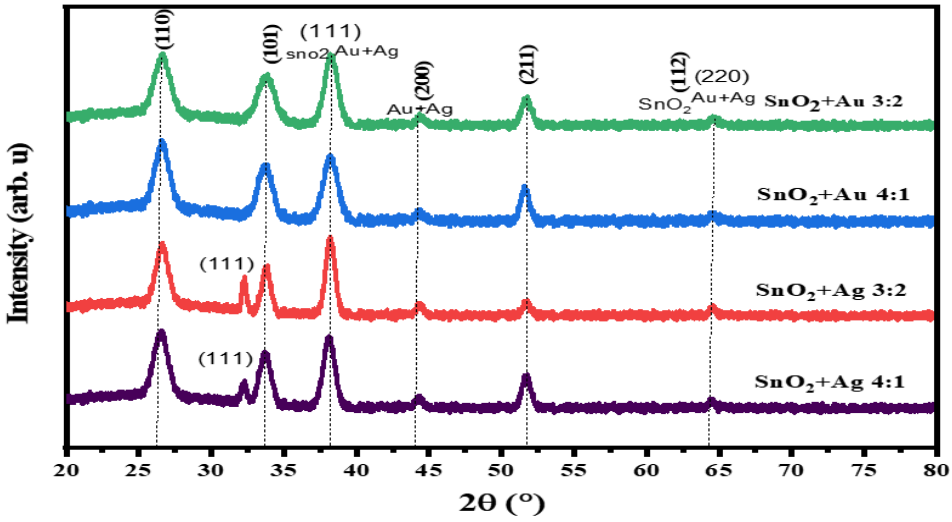

Figure 4: X-Ray diffraction of SnO_2 films incorporated with gold and silver NPs.

Table 1: Structural parameters for SnO_2+Ag at different volume ratios (4:1 and 3:2).

Sample	2 θ (°)	FWHM (rad)	D_{hkl} (nm)	Strain×10^{-3}	d-Spacing (Å)	a,c (Å)
SnO_2+Ag (4:1)	26.632	0.0164	9.0	17.413	3.344	a=4.729 c=3.442
	32.134	0.0034	43.8	2.981	2.783	
	33.842	0.0048	31.4	3.951	2.646	
	37.973	0.0061	24.7	4.491	2.367	
	44.324	0.0096	16.2	5.902	2.041	
	51.679	0.0109	14.6	5.674	1.767	
	64.479	0.0048	35.6	1.905	1.443	
SnO_2+Ag (3:2)	26.780	0.0048	30.9	5.049	3.326	a=4.703 c=3.444
	32.175	0.0048	31.3	4.168	2.779	
	33.864	0.0054	27.5	4.513	2.644	
	38.141	0.0082	18.5	5.961	2.357	
	44.363	0.0055	28.4	3.369	2.040	
	51.693	0.0055	29.2	2.836	1.766	
	64.460	0.0068	24.9	2.724	1.444	

Table 2: Structural parameters for SnO_2+Au at different volume ratios (4:1 and 3:2).

Sample	2 θ (°)	FWHM (rad)	D_{hkl} (nm)	Strain×10^{-3}	d-Spacing (Å)	a,c (Å)
SnO_2+Au (4:1)	26.614	0.0164	9.0	17.425	3.346	a=4.732 c=3.192
	33.838	0.0055	27.5	4.516	2.646	
	38.125	0.0048	37.1	2.982	2.358	
	44.285	0.0109	14.2	6.753	2.043	
	51.605	0.0054	29.2	2.841	1.769	
	64.413	0.0068	24.9	2.726	1.445	
SnO_2+Au (3:2)	26.614	0.0164	9.0	17.322	3.345	a=4.731 c=3.196
	33.810	0.0164	9.1	13.561	2.648	
	38.137	0.0048	37.1	2.981	2.357	
	44.359	0.0109	14.2	6.740	2.040	
	51.678	0.0082	19.5	4.255	1.767	
	64.415	0.0068	24.9	2.726	1.445	

The lattice constants for the SnO_2-Au and SnO_2-Ag composite films closely match the standard values of the tetragonal rutile structure, with a = 4.738 Å and c = 3.187 Å, respectively.

A noticeable increase in crystallite size was observed as the concentration of Au and Ag nanoparticles increased. Furthermore, the enhancement in crystallite size was more significant for SnO_2+Ag films compared to SnO_2+Au, consistent with previous findings reported in the literature [21].

The lattice parameters of SnO_2 doped with gold and silver closely match the standard values for its tetragonal structure (a = 4.738 Å, c = 3.187 Å). It is also observed that the crystallite size grows as the concentration of Au and Ag nanoparticles increases. In the case of (SnO2 +Ag NPs) the crystalline size increase more than that of (SnO2 +Au NPs). The results are in agreement with other reports [21].

3.3 Optical Properties

Figure 5 illustrates the absorption coefficient as a function of photon energy for SnO_2 thin films and SnO_2 films incorporated with Au and Ag nanoparticles at different volumetric ratios (3:2 and 4:1).

The absorption coefficient increases gradually with increasing photon energy and reaches values on the order of 10^4 cm^{-1} near the fundamental absorption edge. Such high values indicate that the films exhibit direct allowed electronic transitions.

It is also observed that the absorption coefficient of the films containing Au nanoparticles is higher than that of the films incorporated with Ag nanoparticles, which suggests stronger interaction between photons and charge carriers in the Au-based composites [15], [17], [22].

To determine the optical band gap of the prepared thin films, a graphical method based on the relationship between the absorption behavior and photon energy was used, as shown in Figure 6. The band gap values were extracted from the extrapolation of the linear portion of the spectral dependence, as commonly applied for semiconducting materials.

Figure 6 presents the optical band gap results for SnO_2 films (0.5 M) incorporated with gold and silver nanoparticles at different volume ratios (3:2 and 4:1). The calculated band gap values were 2.46, 3.56, 3.58, 3.80, and 3.85 eV, respectively.

It is evident that the band gap decreases with increasing nanoparticle content in the SnO_2 matrix. In addition, films containing Ag nanoparticles show slightly higher band gap values compared to those containing Au nanoparticles [10], [23], [24].

3.4 Gas Sensor Result

Figure 7 illustrates the gas sensitivity of pure SnO_2, SnO_2+Au (3:2), and SnO_2+Ag (3:2) sensors deposited on glass substrates as a function of operating temperature (150, 200, 250, and 300 °C). The tests were conducted using a reducing gas (NH_3, 30 ppm).

The pure SnO_2 sensor exhibited the highest sensitivity toward 30 ppm of NH_3, with air-mixed response ratios at operating temperatures up to 250 °C of approximately 24.94%, 12.5%, and 2.47% for pure SnO_2, SnO_2+Ag (3:2), and SnO_2+Au (3:2), respectively.

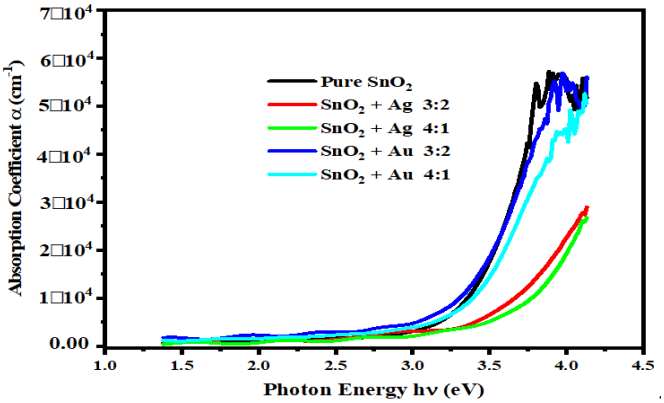

Figure 5: The absorption coefficient as a function of the photon energy for SnO_2 thin films incorporated with gold and silver NPs at different volume ratios.

These observations indicate a marked enhancement in the gas sensing performance of SnO_2-based sensors toward reducing gas. The improved sensitivity can be attributed to the nanostructured SnO_2 grains on the substrate, which increase the surface area available for oxygen adsorption.

When the grain size of SnO_2 becomes comparable to the subsurface depletion layer thickness, the resistance and sensitivity of the sensor are predominantly governed by the grain structure itself. Furthermore, the results reveal that sensitivity rises with increasing operating temperature, a trend consistent with the temperature-dependent conductivity of semiconductors.

At elevated temperatures, more electrons are thermally excited from shallow donor levels; typically created by oxygen vacancies; into the conduction band, thereby enhancing gas adsorption and charge transfer processes [25].

Figure 8 illustrates the response and recovery times of the gas sensors as a function of operating temperature for NH_3 gas. Measurements were carried out at a bias voltage of 3 V within the temperature range of 150–300 °C. The results clearly indicate that both response and recovery times decrease as the operating temperature increases, demonstrating enhanced sensor kinetics at higher temperatures. For NH_3 detection, the SnO_2+Ag (3:2) sensor exhibited the longest response time of 11.7 s at 150 °C, whereas the SnO_2+Au (3:2) sensor showed the longest recovery time of 31.5 s at 200 °C. These results suggest that operating temperature plays a crucial role in determining the dynamic response characteristics of SnO_2-based sensors, where increased temperature accelerates adsorption and desorption processes, leading to faster response and recovery behavior [26], [27].

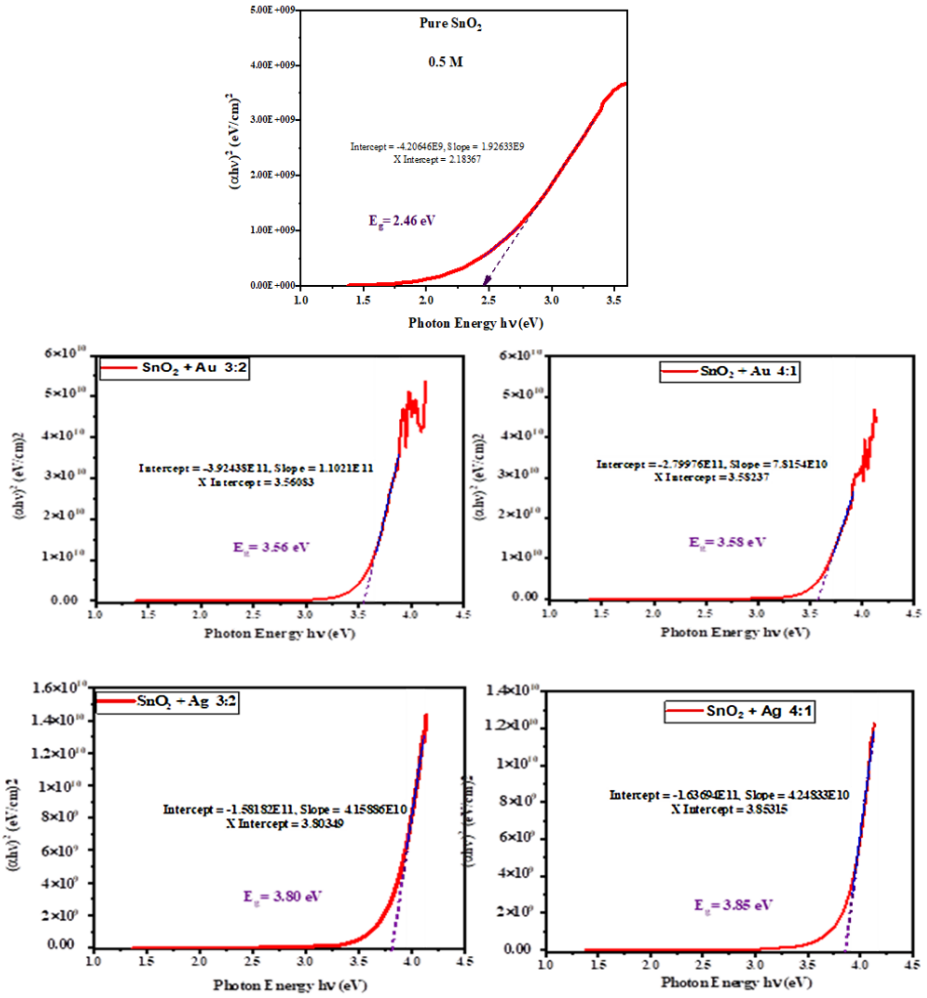

Figure 6: Energy band-gap of SnO_2 films incorporated with gold and silver NPs.

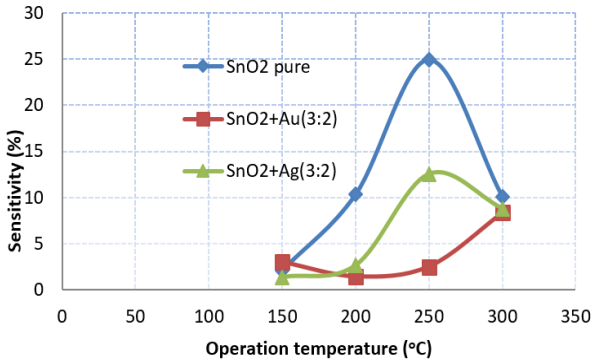

Figure 7: The variation of sensitivity with the operation temperature of the prepared SnO_2, SnO_2+Au (3:2), SnO_2+Ag(3:2) to NH_3 gas.

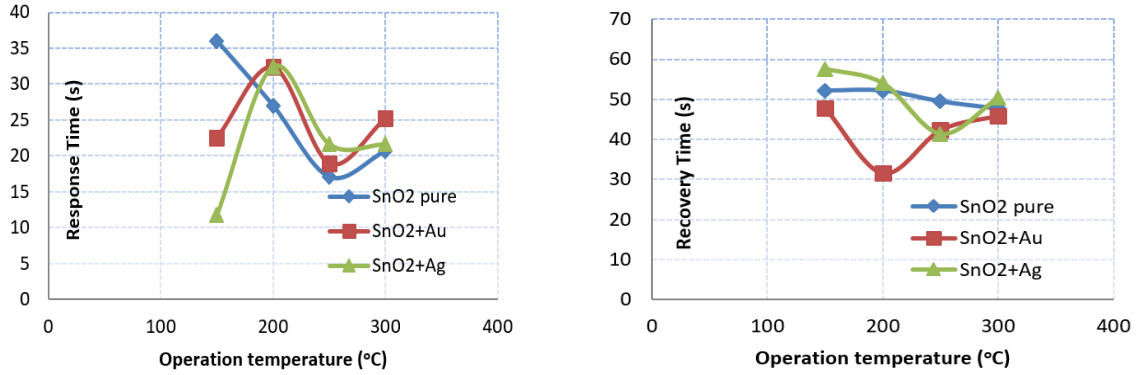

Figure 8: The variation of response time and recovery time with operation temperature of the prepared SnO_2 , SnO_2+Au(3:2), SnO_2+Ag(3:2) gas sensor.

4 CONCLUSIONS

In this work, SnO_2 thin films were fabricated on quartz substrates using the sol–gel spin-coating method. The films were successfully prepared through multiple coating cycles to study the influence of deposition repetition on film properties.

Tin(II) chloride dihydrate ($SnCl_2 \cdot 2H_2O$) served as the precursor material, 2-methoxyethanol was used as the solvent, and monoethanolamine (MEA) acted as the stabilizing agent. Gold (Au) and silver (Ag) nanoparticles were synthesized separately using the pulsed laser ablation in liquid (PLAL) technique with a Q-switched Nd:YAG laser operating at 1064 nm wavelength, 520 mJ pulse energy, 1 Hz repetition rate, and 450 pulses.

The SnO_2 precursor solution was then mixed with the Au and Ag colloids in volumetric ratios of 3:2 and 4:1, respectively. The surface morphology of the resulting nanocomposite films was analyzed using field emission scanning electron microscopy (FE-SEM), while their optical characteristics were examined via UV–Vis spectroscopy.

X-ray diffraction (XRD) patterns revealed six principal peaks: four at (110), (101), (211), and (112), which correspond to the tetragonal rutile phase of SnO_2, and two additional peaks at (200) and (220), attributed to the cubic crystalline phases of Au and Ag nanoparticles. A shared (111) reflection was also detected for both SnO_2 and the metallic nanoparticles.

Optical studies demonstrated a reduction in the band-gap energy (3.85–3.56 eV) with increasing concentrations of Au and Ag nanoparticles within the SnO_2 matrix. Among all samples, the SnO_2+Au (3:2) composite exhibited the best NH_3 gas-sensing performance, exhibiting high sensitivity with rapid response and recovery times. The optimum operating temperature of 300 °C, at which the best gas-sensing response was observed. temperatures.

REFERENCES

[1] G. E. Patil et al., "Synthesis, characterization and gas sensing performance of SnO_2 thin films prepared by spray pyrolysis," Bull. Mater. Sci., vol. 34, no. 1, pp. 1–9, 2011, doi: 10.1007/s12034-011-0048-0.

[2] L. C. Nehru, V. Swaminathan, and C. Sanjeeviraja, "Photoluminescence studies on nanocrystalline tin oxide powder for optoelectronic devices," Am. J. Mater. Sci., vol. 2, no. 2, pp. 6–10, 2012, doi: 10.5923/j.materials.20120202.02.

[3] M. Shaik, P. R. Reddy, and B. R. Ravuri, "Structural, optical, and electrical properties of SnO_2 nanoparticles synthesized by a co-precipitation route," J. Mater. Sci. Mater. Electron., vol. 32, pp. 14818–14830, 2021, doi: 10.1007/s10854-021-06126-4.

[4] G. W. Hunter, C. C. Liu, and D. D. Makel, MEMS Handbook: Design and Fabrication, 2nd ed. Boca Raton, FL, USA: CRC Press, 2006.

[5] W. J. Albery and M. D. Archer, "Optimum efficiency of photogalvanic cells for solar energy conversion," Nature, vol. 270, pp. 399–402, 1977, doi: 10.1038/270399a0.

[6] S. Ferrere, A. Zaban, and B. A. Gregg, "Dye sensitization of nanocrystalline tin oxide by perylene derivatives," J. Phys. Chem. B, vol. 101, pp. 4490–4493, 1997, doi: 10.1021/jp970699u.

[7] P. G. Harrison, C. Bailey, and W. J. Azelee, "Studies in surface science and catalysis," J. Catal., vol. 186, pp. 147–149, 1999, doi: 10.1006/jcat.1999.2557.

[8] Y. S. He, J. C. Campbell, R. C. Murphy, M. F. Arendt, and J. S. Swinnea, "Electrical and optical characterization of Sb:SnO_2," J. Mater. Res., vol. 8, no. 12, pp. 3131–3134, 1993, doi: 10.1557/JMR.1993.3131.

[9] S. K. Mishra, P. Maiti, and S. K. Singh, "Influence of particle size and surface area on the gas sensing properties of SnO_2 nanoparticles," J. Mater. Sci. Mater. Electron., vol. 31, pp. 11056–11067, 2020, doi: 10.1007/s10854-020-03611-4.

[10] M. X. Sun, W. Liu, J. Xu, and G. Lu, "Recent advances in SnO_2-based gas sensors: A review," J. Mater. Sci. Mater. Electron., vol. 31, pp. 3115–3134, 2020, doi: 10.1007/s10854-020-02835-9.

[11] P. Sen et al., "Preparation of Cu, Ag, Fe and Al nanoparticles by the exploding wire technique," Proc. Indian Acad. Sci. (Chem. Sci.), vol. 115, pp. 499–508, 2003, doi: 10.1007/BF02708293.

[12] M. Shah et al., "Gold nanoparticles: various methods of synthesis and antibacterial applications," Front. Biosci., vol. 19, pp. 1320–1344, 2014, doi: 10.2741/4284.

[13] G. Yang, Laser Ablation in Liquids: Principles and Applications in the Preparation of Nanomaterials, 1st ed. Singapore: Pan Stanford Publishing, 2012.

[14] Sharma et al., "Synthesis of Au–SnO_2 nanoparticles for electrochemical determination of vitamin B_{12}," J. Mater. Res. Technol., vol. 9, no. 6, pp. 14321–14337, 2020, doi: 10.1016/j.jmrt.2020.10.089.

[15] M. Aziz, S. S. Abbas, and W. R. Wan Baharom, "Size-controlled synthesis of SnO_2 nanoparticles by sol–gel method," Mater. Lett., vol. 91, pp. 31–34, 2013, doi: 10.1016/j.matlet.2012.09.097.

[16] H. Li et al., "Optically tunable tin oxide–coated hollow gold–silver nanorattles for use in solar-driven applications," ACS Omega, vol. 5, pp. 23769–23777, 2020, doi: 10.1021/acsomega.0c03159.

[17] Z. Obeizi et al., "Synthesis and characterization of Ag–SnO_2 nanoparticles and investigation of their antibacterial and antibiofilm activities," J. New Technol. Mater., vol. 10, no. 2, pp. 10–17, 2020, doi: 10.12816/0058531.

[18] Z. T. Khodair, N. A. Bakr, A. M. Hassan, and A. A. Kamil, "Influence of substrate temperature and thickness on structural and optical properties of CZTS nanostructure thin films," J. Ovonic Res., vol. 15, no. 6, pp. 377–385, 2019.

[19] A. A. Mohammed et al., "Effect of vanadium doping on structural properties of SnO_2 nanoparticles prepared by sol–gel method," AIP Conf. Proc., vol. 2475, p. 090001, 2023, doi: 10.1063/5.0140909.

[20] Aryanto et al., "Effect of annealing on optical properties of zinc oxide thin films prepared by homemade spin coater," J. Phys.: Conf. Ser., vol. 817, p. 012025, 2017, doi: 10.1088/1742-6596/817/1/012025.

[21] P. Khaenamkaew, D. Manop, C. Tanghengjaroen, and W. P. Na Ayuthaya, "Crystal structure, lattice strain, morphology, and electrical properties of SnO_2 nanoparticles induced by low calcination temperature," Adv. Mater. Sci. Eng., Article ID 3852421, 2020, doi: 10.1155/2020/3852421.

[22] J. Mullerova and P. Sutta, "On some ambiguities of the absorption edge and optical band gaps of amorphous and polycrystalline semiconductors," Commun. Sci. Lett. Univ. Zilina, vol. 19, no. 3, pp. 9–15, 2017.

[23] M. I. Khan et al., "Characterizations of multilayer ZnO thin films deposited by sol–gel spin coating technique," Results Phys., vol. 7, pp. 651–655, 2017, doi: 10.1016/j.rinp.2017.01.026.

[24] D. Mulmi, A. Dhakal, and B. R. Shah, "Effect of annealing on optical properties of zinc oxide thin films prepared by homemade spin coater," Nepal J. Sci. Technol., vol. 15, no. 2, pp. 111–116, 2014.

[25] X. Pan, X. Zhao, J. Chen, A. Bermak, and Z. Fan, "A fast-response/recovery ZnO hierarchical nanostructure-based gas sensor with ultra-high room-temperature output response," Sens. Actuators B Chem., vol. 206, pp. 764–771, 2014, doi: 10.1016/j.snb.2014.09.015.

[26] Y. Liu, E. Koep, and M. Liu, "A highly sensitive and fast-responding SnO_2 sensor fabricated by combustion chemical vapor deposition," Chem. Mater., vol. 17, pp. 3997–4000, 2005, doi: 10.1021/cm050644i.

[27] M. Latino and G. Neri, "Chemoresistive metal oxide gas sensors: working principles and applications," AAPP – Atti Accad. Peloritana Pericolanti, vol. 98, no. S1, Article A41, 2021, doi: 10.1478/AAPP.98S1A41.